Innovative 3D Printed Coil and Cooling Designs for Weight-Sensitive Energy-Saving Electrical Machine

Ahmed Selema [1,2,3*], (Member, IEEE), Joffrey Van Den Abbeele [1,2],
Mohamed N. Ibrahim [1,2,4], (Senior Member, IEEE), and Peter Sergeant [1,2], (Senior Member, IEEE)

[1] *Department of Electromechanical, Systems, and Metal Engineering, Ghent University, 9000 Ghent, Belgium*

[2] *FlandersMake@UGent, Core Lab MIRO, 3001 Leuven, Belgium*

[3] *Department of Electrical Engineering, Faculty of Engineering, Menoufia University,32511 Menoufia, Egypt*

[4] *Department of Electrical Engineering, Kafrelshiekh University, 33511 Kafrelshiekh, Egypt*

* Corresponding author: Ahmed Selema (ahmed.selema@ugent.be; selema@ieee.org)

***Abstract*— The performance of electrical machines is often limited by manufacturability challenges. With the emergence of additive manufacturing (AM) technology, new design solutions that were previously impossible using conventional production techniques are becoming applicable. This work addresses novel design possibilities in the manufacturing of machine windings. Using AM technology, a series of 3D-printed coils are designed and prototyped for high-power density electrical machines. The power losses of these new coils are measured and compared with the conventional windings. The 3D coil designs combine higher performance and easier manufacturability. Moreover, a new thermal management concept is introduced using novel AM-shaped profile coils with direct cooling channels featuring ridged surfaces. The cooling tubes have small grooves or ridges on their surface that create a series of indents, which help increase their surface area and improve their cooling efficiency. The dimensions of the proposed heat exchanger are optimized to achieve a good balance between the current density and the cooling performance. The investigation includes identifying suitable materials for both the coils and the heat exchanger that can enhance the electromagnetic and thermal performance of the electrical machine while achieving a lightweight structure. Finally, the experimental results demonstrate the effectiveness of the proposed approach in achieving significant improvements in performance and weight reduction. Compared to the conventional copper coils, the new design has twice the current carrying capacity with only 53% weight.**

Keywords*— *Electrical machines, 3D printing, Thermal management, Manufacturability.

I. INTRODUCTION

A. Manufacturability Challenges for EVs

As the market of electric vehicles (EVs) expands, high reliability and ease of manufacturability are becoming important aspects during the early stage design process of electric traction motors. Therefore, original equipment manufacturers (OEMs) are trying to address manufacturability challenges using unconventional production techniques that allow for improved supply chain resiliency. In this context, additive manufacturing (AM) technology has gained a lot of interest recently [1], [2]. Thanks to its unique design freedom, complex and scalable parts can be easily printed for electrical machines saving a lot of time and cost. Additionally, with the high feedstock flexibility, advanced lightweight materials can be used with tuned chemical composition. To sum up, the development of electrical machines can be greatly accelerated using AM technologies, resulting in redesign of traditional manufacturing as well as rapid commercialization of new families of electrical machines [3]–[5].

B. Weight Saving in Electrical Machine

Weight saving and power density boosting are crucial considerations in the design of electrical machines as vehicle electrification advances. It can allow for more compact machine designs, making them more suitable for use in tight spaces. In [6], [7], the masses of all the components in the electric motor are investigated for lightweight electric drives and traction applications. Also, the weight distribution of an electrical machine is outlined as shown in Fig. 1. As can be seen, both the stator and the housing possess nearly 80% of the total machine weight. That is why the mass reduction of stator windings and cooling jacket is of importance for all kinds of electric machines since a lower weight allows reduced energy consumption, better dynamic response, and higher power density, while also reducing the material and manufacturing costs.

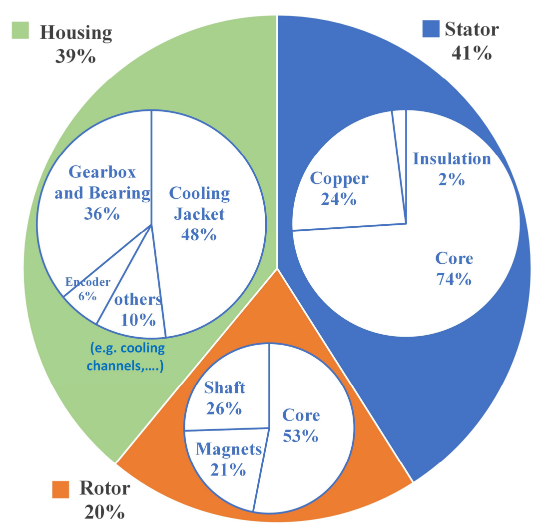

Fig. 1. Weight distribution of a PM electrical machine with a cooling jacket [6], [7].

C. Limitations of Conventional Windings

One of the common electrical machines that can benefit from AM technology is the switched reluctance machine (SRM). In such machine, multi-turn concentrated coils are typically used for the stator three-phase windings. A case study is shown in Fig. 2 for a 6.5 kW peak, 4 kW continuous

3-phase SRM with slot/pole combination of 6/4 slot. The main specifications are listed in Table I. One of the main issues of SRMs is the lower copper utilization leading to lower efficiency and reduced power density. To tackle this issue, different cooling system can be used to dissipate the heat generated in the winding conductors. A naturally air-cooled jacket with fins has a simple and rugged structure. However, it is not as effective as the water cooling systems (whether direct or indirect). In the baseline machine (Fig. 2), the 26-turn coils are typically wound first using a single strand round conductor and then placed in the slot. As a result, there is a triangular prism gap between adjacent windings. This space is used for direct cooling of the coil conductors and to push current limitations to higher levels. Nevertheless, the slot copper fill factor is minimally reduced by 25% due to this space [8]. Finally, the limitations in such traditional windings are summarized as follows;

- Low fill factor
- High resistance
- High weight
- Bad thermal performance
- High eddy current losses
- Low eco-efficiency/ recyclability

Addressing these challenges requires interdisciplinary research, including advancements in materials, design techniques, and manufacturing process. Overcoming these challenges will contribute to the wider adoption of SRMs in various industries, enabling improved performance, energy efficiency, and weight saving.

D. Additive Manufacturing (AM) for Electromagnetic Parts

Different research studies highlighted very promising outcomes of using AM technology for electrical machines. In [9], state of the art of additively manufactured electromagnetic materials is introduced for weight-optimized electrical machines. It is found that printing of magnetically and electrically conductive materials show equivalent properties to high-grade commercial materials [10]–[14]. Moreover, It is also possible to print passive parts for electrical machines with high mechanical properties and optimized weight. An example is reported in [15] for a complete electrical drive housing produced by Porsche. This housing has double the mechanical strength and 40% lighter than the conventional design. In parallel, AM hard magnetic materials are introduced in [16], [17]. Roughly equivalent performance is obtained compared to commercial ferrite permanent magnets (PMs). Nevertheless, printed high quality PMs are still at early-stage research [18]. To achieve that, an effective magnetization process is yet needed to impart complex 3D printed PMs. On the counterpart, the maturity of AM electrically conductive materials is superior in many ways. That is why 3D printed coils are employed in many applications, and even suitable for commercial applications. In [19], [20], pure copper coils are printed with a relative electrical conductivity of 100% IACS. Yet, due to the relatively higher production costs, printing pure copper is still limited to nonconventional complex winding types [21]. Alternatively, aluminum alloys can be used for such windings due to their lower weight as well as cost [22]–[29].

In [30], a novel approach involving a 3D printed passive insert has been introduced. This insert piece serves to encapsulate the stator end-windings, resulting in an augmented level of contact between the end-windings and the machine housing, as depicted in Fig. 3. To enhance thermal conductivity, axial extensions have been incorporated, effectively occupying the triangular space that typically remains unused between two adjacent coils. This innovative approach has led to a significant improvement in thermal performance, and the current density has been by over 30%. This remarkable enhancement can be attributed to the utilization of extended end-winding cooling inserts. Yet, this cooling system is exclusively compatible with conventional copper coil, limiting its applicability in machines featuring other materials or winding configurations.

With this being said, this paper introduces unconventional design solutions for the manufacturing of machine windings enabled by AM technology as shown in Fig. 4. Furthermore, a new direct cooling approach is proposed using a novel AM shaped profile coil and heat exchanger which allow for high electromagnetic performance as well as optimal thermal management.

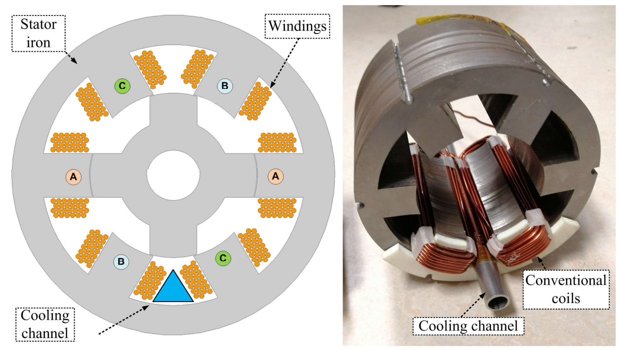

Fig. 2. Configuration of a typical three-phase switched reluctance machine with direct cooling channels.

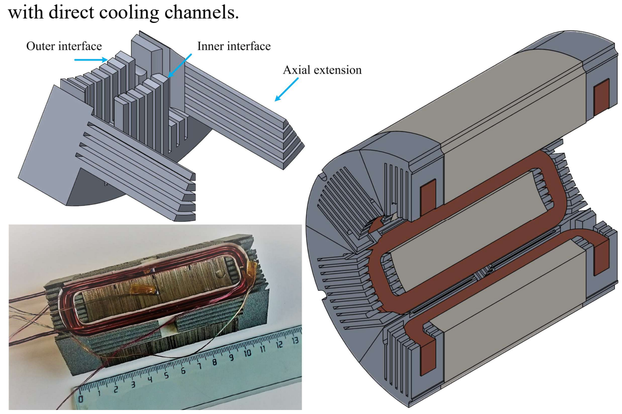

Fig. 3. Additively-printed inserts with internal heat extraction fins for end-winding passive cooling [30].

TABLE I.
GEOMETRICAL AND ELCTROMAGNETIC PARAMETERS OF THE SWITCHED RELUCTANCE MACHINE.

Parameter	Value	Parameter	Value
Number of slots	6	Number of rotor poles	4
Stator outer diameter	120 mm	Number of Turns per coil	26
Stator inner diameter	62.5 mm	Rated Power	6.5 kW
Tooth width	17.5 mm	Rated MMF per coil	910 AT
Stack length	78.5 mm	Core material	NO20
Rotor outer diameter	61.8 mm	Base speed	3000 RPM
Rotor inner diameter	40 mm	Nominal frequency	100 Hz

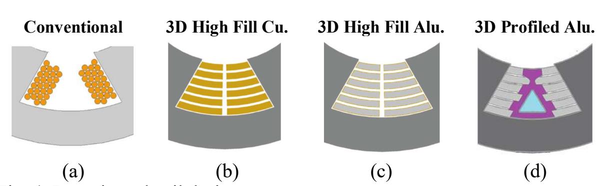

Fig. 4. Investigated coil designs.

II. 3D Printed Coils with High Fill Factor

To combine a high fill factor and good thermal performance, a 3D trapezoidal-shape coil is proposed as shown in Fig. 5. This 6-turn coil has conductors with different cross-sections to have a perfect fit in the trapezoidal slot. Also, the coil has a very high fill factor of 73% which is two times the value in the conventional coils. Moreover, the end turns are ingenuously designed to have a smooth and continuous transition between the different cross-sections. In order to apply this concept to a SRM, the stator must have a partitioned structure that can be assembled later after all coils are inserted. Additionally, the thermal management system will be using an outer cooling jacket with indirect water cooling.

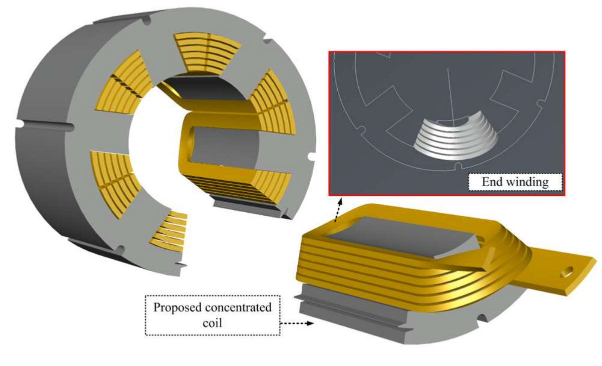

Fig. 5. High fill factor trapezoidal-shape coil. (a) 3D design, (b) 3D printed prototype using aluminum.

Different materials and methods can be used to print the aforementioned coil design. Apart from copper, a cost-effective alternative will be using aluminum. Despite aluminum has lower electrical conductivity, it has nearly half weight and much lower cost compared to copper. Using transient finite element analysis (FEA), the power losses are calculated at different rotor speeds for the conventional coil. The results are also compared with a trapezoidal-shape coil with two different materials (copper and aluminum) at different frequency levels as shown in Fig. 6. It is found that at nominal frequency level, using aluminum coil reduces the losses by over 25%. Also, in case of copper, the losses decrease by over 50%. Therefore, it can be concluded that using a 3D printed trapezoidal-shape coil with high fill factor is a more effective replacement for the traditional copper coils.

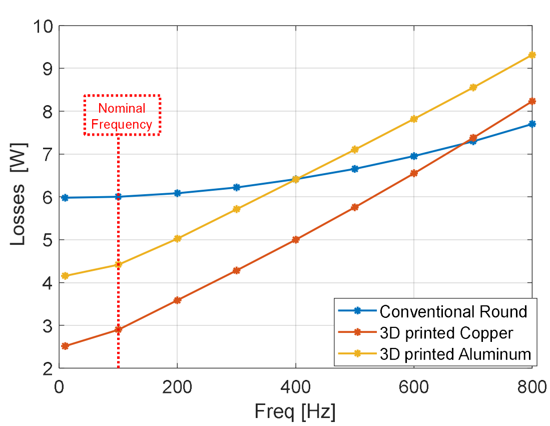

Fig. 6. Average power losses of a single coil at different frequency levels: a comparison between conventional coils and 3D printed ones with high fill factor. (at the same ampere turns value 260AT)

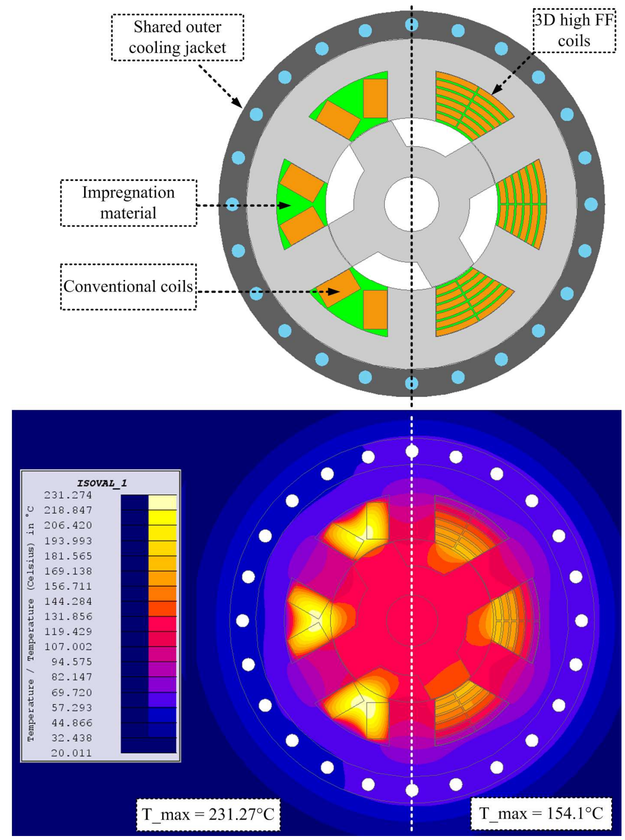

Fig. 7. Thermal profile of the 3D high fill factor coil compared conventional coils under the same cooling conditions. (Ampere turns value = 1080AT)

The thermal profile of this design is compared with the conventional coils as shown in Fig. 7. To save simulation time, the stator is divided into two parts which are thermally isolated, yet, electromagnetically coupled. This was simulated by creating a thermal isolating line between the two halves that prevent heat flow from one to another. For a fair comparison between both coil designs, both conventional and 3D coils share the same outer cooling jacket and cooling conditions. Under the same value of ampere turns, it is found the 3D high fill aluminum coils has remarkably lower temperature compared to the conventional coils. Therefore, the trapezoidal-shape coil is 3D printed using aluminum alloy.

III. Indented Direct Cooling Tube Concept

The current density distribution is simulated for the 3D high fill coil as shown in Fig. 8. In order to push current limitations to higher levels, direct cooling channels are usually used to effectively extract the heat generated in the middle of the slot. This direct cooling approach can also save a major part of the machine weight and volume, because the cooling channels are more compact and much lighter compared to outer cooling jacket. In [31], using direct in-winding cooling allows for a significant increase of current density limit by 30% compared to the naturally air-cooled SRM. Yet, the conventional triangular-shape cooling channel is not the optimal design for direct cooling. The main reason is that it has a very limited contact surface especially if the multi-turn windings have traditional round conductors. So, the contact surface between the turn and the channel is a line rather than an area as shown in Fig. 9. As a result, they are not as effective as expected in removing losses from windings.

For an optimal heat dissipation, the contact surface needs to be increased. To this aim, a novel grooved-profile coil is introduced in Fig. 9. In such design, the individual turns have unequal widths allowing for a zigzag-surface heat exchanger. The cooling tube has small grooves or ridges on its surface that create a series of indents, which help increase the surface area and improve its cooling efficiency. The proposed design has much larger contact surface area compared to the conventional triangle shape cooling channel. Additionally, the curved bottom of the cooling channel leads to an improved contact with the stator body.

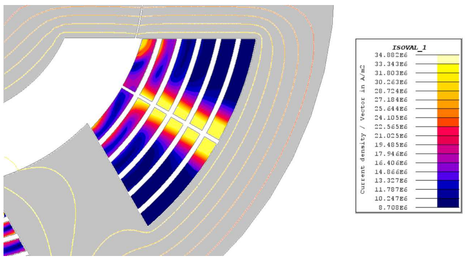

Fig. 8. Localized current density distribution for the 3D high fill coil.

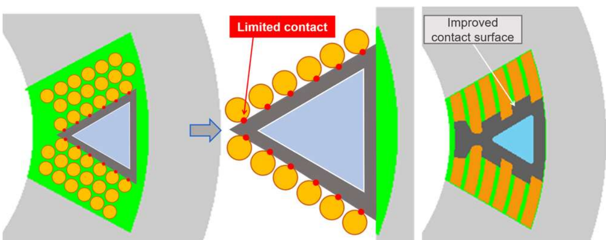

Fig. 9. Main concept for the 3D zigzag-shaped profile heat exchanger.

To save time during the transient thermal simulation, the proposed design is solved with the conventional coils on the same stator core as shown in Fig. 10(a). As can be seen, two 3D shaped coils are thermally simulated at stranded level, which are Coils A, B. On the opposite side, two conventional coils (Coils a, b) are also defined as heat sources. In between, dummy coils (C, c) are used to complete the electrical circuit without being defined as heat source.

Different materials can be used for the heat exchanger such as aluminum or stainless steel. Given its low mass density and high thermal conductivity, aluminum is initially selected as the simulation material of both heat exchangers. In this thermal simulation, the winding losses and the iron losses are defined as the main sources of the power losses. The heat exchanger is defined as a thermally conducting material without any electrical conductivity. Thus, any induced eddy losses in the heat exchanger are not considered, and the cooling channel is not defined as a possible heat source. As a result, there is an over-optimistic results when aluminum is selected. Yet, practically speaking, the eddy current losses in aluminum can cause higher temperatures.

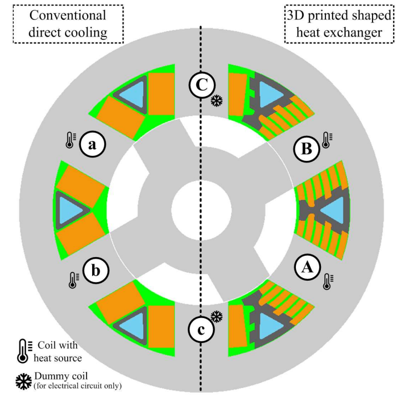

(a)

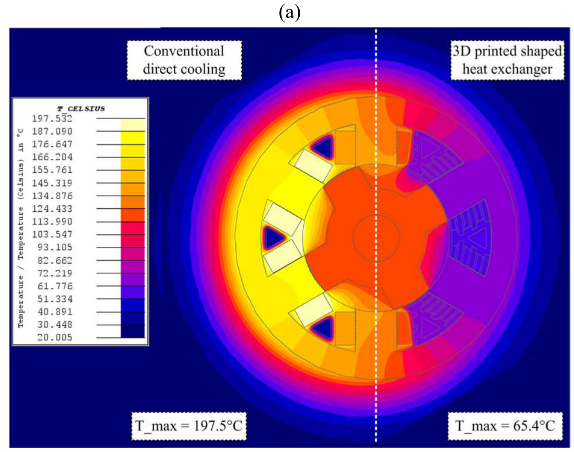

(b)

Fig. 10. Grooved-profile coil with the zigzag-surface heat exchanger compared to conventional direct cooling. (a) Design concept, (b) Thermal profile under the same operating conditions.

A comparison between the thermal performances is also shown in Fig. 10(b) under the same ampere turns and coolant flow rate values. Also, the corresponding instantaneous temperature rise is shown in Fig. 11. As can be seen, the proposed grooved-profile coil along with the zigzag-surface direct cooling channel have remarkably reduced the maximum temperature from 197.5°C to only 65.4°C. Further, the maximum temperature is also compared at different ampere turns and convective heat transfer coefficients as shown in Fig. 12. Obviously, the proposed cooling approach has a much better thermal profile compared to the traditional one under the same operating conditions. This allows for a significant increase of current density. Eventually, the torque and power density will be improved.

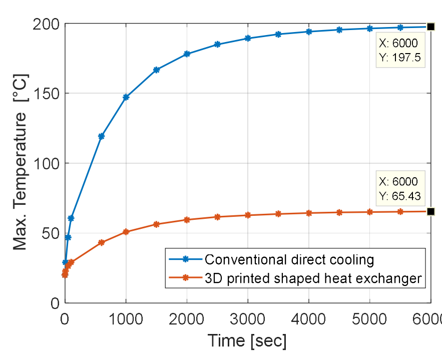

Fig. 11. Comparison between the instantaneous temperature rise at a fixed convective heat transfer coefficient (h=1000 W/m^2.°C), and Ampere turns = 1080AT.

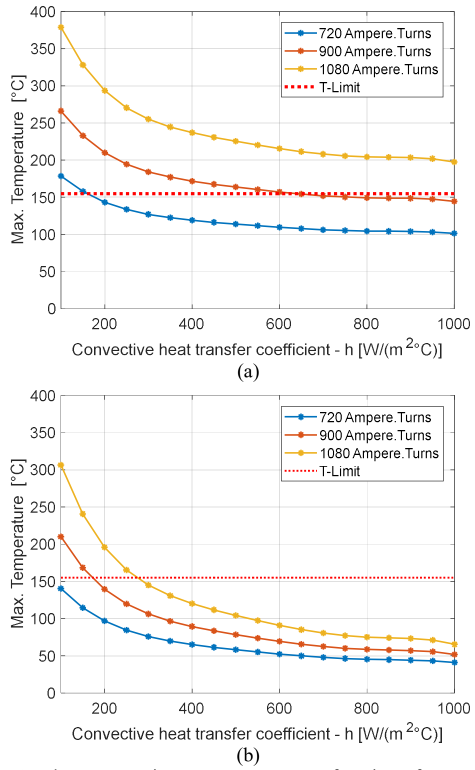

Fig. 12. Steady state maximum temperature as function of convective heat transfer coefficient at different ampere turns levels. (a) Conventional direct cooling. (b) 3D grooved-profile coil with the zigzag-surface heat exchanger.

IV. Heat Exchanger Optimization

The dimensions of the heat exchanger are optimized to have a good balance between the current density and the cooling performance. In order to achieve that, an advanced parametric model is created for the zigzag heat exchanger. The main dimensions of the heat exchanger are shown in Fig. 13, and their specifications are listed in Table II. The zigzag design is also compared with an initial design without any grooves, and different shapes of the cooling channel are investigated including the circular and triangular shapes. The heat transfer coefficient is calculated in the simulation algorithm using Gnielinski correlation for enhanced tubes [32]. The optimization flow chart is shown in Fig. 14. The thermal and electromagnetic performances are co-simulated under different cooling designs targeting maximum current density and minimum power losses. Further, the temperature constraint are defined at a fixed level of 155°C. The total number of simulated designed is 2000. Nearly 45% of these samples have passes the temperature criteria. The scatter diagram of the current density versus the power losses is shown in Fig. 15 at different cooling design and conditions. The best-in-class samples are marked with high current density as well as low power losses.

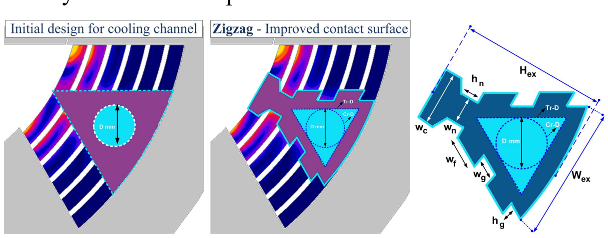

Fig. 13. The main dimensions of the zigzag heat exchanger.

TABLE II.
MAIN DIMENSIONAL SPECIFICATIONS OF THE HEAT EXCHANGER

Height of the heat exchanger	$\boldsymbol{H_{ex}}$
Width of the heat exchanger	W_{ex}
Cooling channel diameter	D
Cooling channel Type: Circular	$Cr - D$
Cooling channel Type: Triangular	$Tr - D$
Cooling rate [W/(m2 °C)]	h
Cooling type	*water*
Groove width	w_g
Groove height	h_g
Fin width	w_f
Neck width	w_n
Neck height	h_n
Cap width	w_c

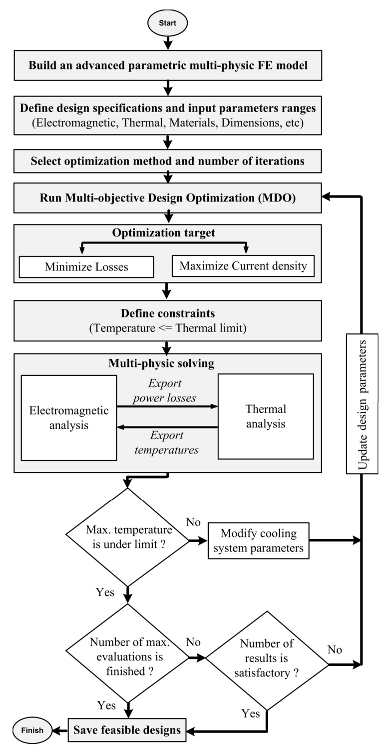

Fig. 14. Optimization flow chart for heat exchanger dimensions.

The optimal dimensions are selected for the heat exchanger. The ideal design has an outer circumference length of 74.4mm, which is nearly twice the length of the initial design (38.7mm). Furthermore, a comparison between the optimal design and the initial one is shown in Fig. 16 under the highest current density value obtained from the optimization. Also, the maximum temperature is compared for different cooling channel sizes and shapes. When comparing the zigzag design to the initial design, it is evident that the temperature in the initial design exceeds the permissible limit by a significant margin. Moreover, using larger cooling channels results in lower temperatures. Interestingly, the circular cooling channel is not effective for the zigzag shape, while the triangle design efficiently reduces the temperature to within the permissible level. This can be attributed to the fact that the triangle shape provides 65% more surface area compared to the corresponding circular shape ($A_{Tri} = \frac{3\sqrt{3}}{\pi} A_{Cr}$).

Finally, the optimal designs grooved-profile coil along with the zigzag-surface heat exchanger are designed in 3D, and the assembly with the stator are shown in Fig. 17. Different materials can be used for the heat exchanger. The coil samples will be printed from aluminum and the heat exchanger material will be selected as explained in the following sections.

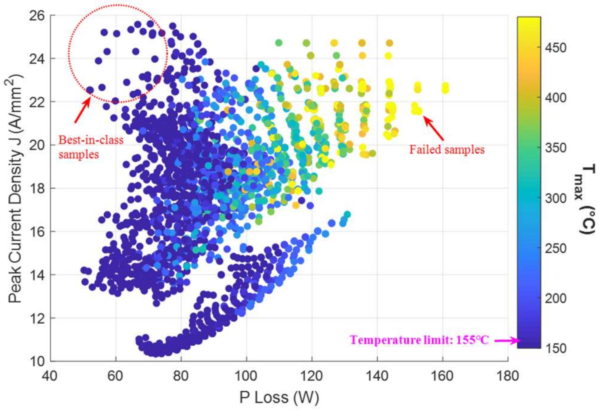

Fig. 15. The scatter diagram of the peak current density versus the power losses at different cooling design and conditions.

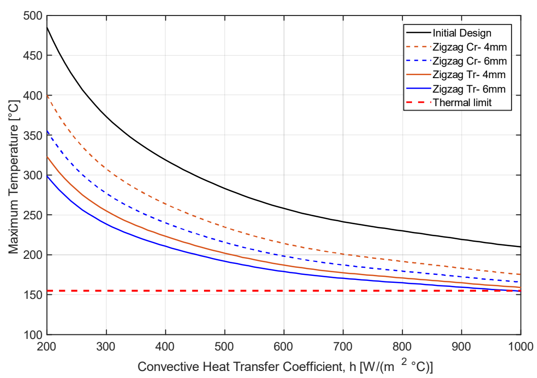

Fig. 16. The maximum temperature as function of convective heat transfer coefficient at the optimal maximum current density.

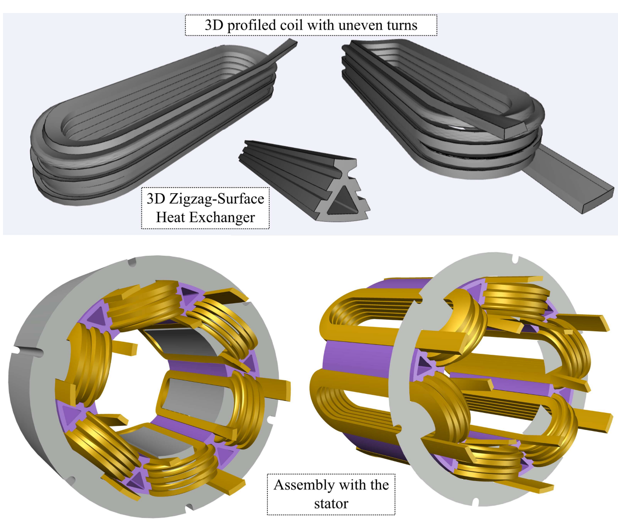

Fig. 17. Assembly of the grooved-profile coil along with the 3D zigzag-surface heat exchanger.

V. Samples Printing and Testing

A. Sample Preparation and 3D Printing

Using selective laser melting (SLM) technology, the trapezoidal-shape high fill factor coil is 3D printed using aluminum alloy ($AlSi_{10}Mg$ powder) with a layer thickness of 50μm as shown in Fig. 18. The turns cross section is gradually decreasing starting from the bottom turn to the upper turn. The final mass density of the built sample is 2670 kg/m^3. The printed part has a very accurate finishing with perfect fit with the core dimensions. Despite having a higher fill factor, the coil is 32% lighter than the conventional copper coil. The combination between low weight and high fill factor qualifies this coil to be used in weight-sensitive high-power density electrical machines without the need for direct cooling. A post-process heat treatment is used to improve the electrical and mechanical properties which is referred to as T6-protocol [33], [34]. After this process, a thin layer of oxidation is formed on the turns surface resulting in a non-electrically conducting surface insulation. As a last step, the coil is dipped in Synthite polyester varnish to ensure no turn-to-turn interconnection.

Using the exact same procedures, the grooved-profile coil is printed using the same materials and the aforementioned steps as shown in Fig. 19. With the uneven conductors, the end turns have a special curvature design to guarantee a smooth transition between turns.

As for the zigzag-shape heat exchanger, aluminum material can provide high thermal conductivity. However, eddy currents can be induced in this passive part causing extra losses and heat. That is why a different material is used as explained in the following section.

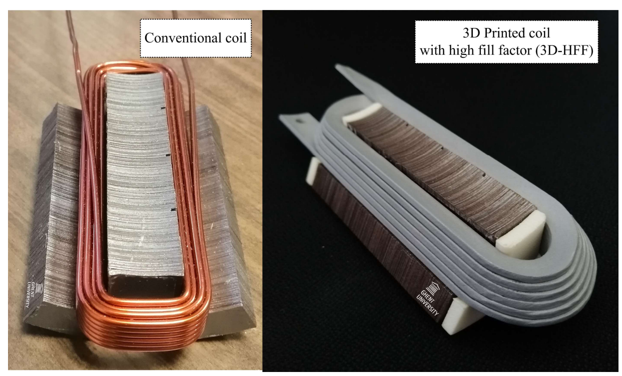

Fig. 18. A motorette with conventional copper coil and 3D printed aluminum coil with high fill factor.

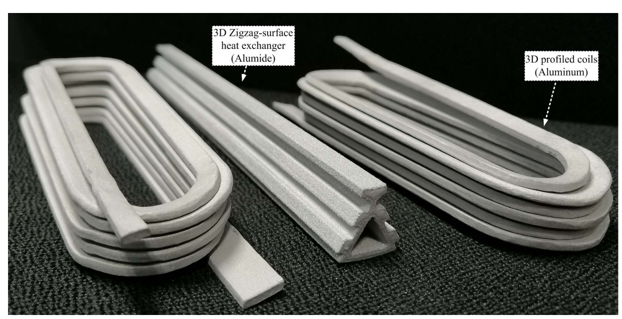

Fig. 19. 3D printing of the grooved-profile coils and the zigzag heat exchanger.

B. *Test Setup and Power Losses*

The winding losses are measured for different samples using the test setup in Fig. 20. It consists mainly out of a DC voltage source, DC-AC inverter, V-I sensors, and data acquisition (DAQ) system. a dSpace MicroLabBox 1202 is used to control the frequency of the AC waveform. Also, an LC filter is used to filter the high order harmonics in the AC output of the inverter and obtain a sinusoidal waveform. Moreover, a thermal camera (GTC400) is used to monitor the temperature of the windings. There is also a multi-channel power analyzer (Tektronix PA4000) used to measure the power losses. A scope (Tektronix TDS3054) is used to monitor the waveforms. Even more, PT100 sensors are used to measure the instantaneous temperate rise and a PCB amplifier is used to send the signal to the DAQ. Finally, the all test sample are connected in series with a water-cooled power resistor to limit any excessive current. The three test samples are explained as follows.

- Coil I: Conventional copper coil. [Fig. 18]
- Coil II: 3D printed trapezoidal-shape aluminum coil with high fill factor [Fig. 18].
- Coil III: 3D printed zigzag-profiled aluminum coil with direct cooling channel [Fig. 19].

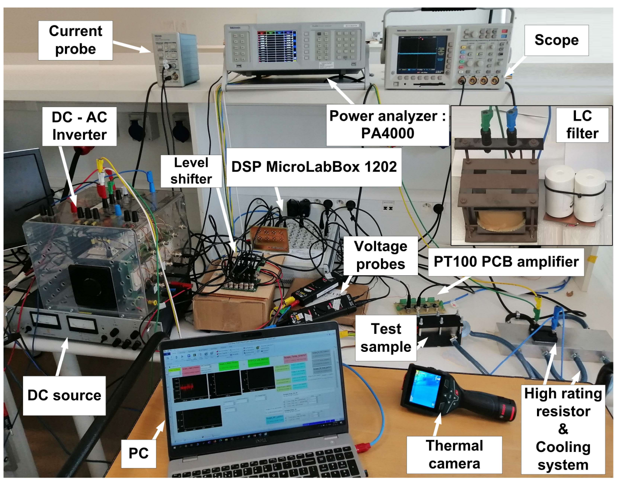

Fig. 20. Test platform for loss measurements of the winding samples.

The power losses are measured for the 3D printed samples and the results are compared with the conventional coils at the same ampere turn level as shown in Fig. 21. As expected, the nominal frequency losses of the high fill aluminum sample (Coil II) are about 25% lower than those in the conventional copper one (Coil I). For the 3D grooved-profile (Coil III), the losses are relatively higher than the Coil II due to the lower fill factor. Yet, it is still has lower losses compared to Coil I at the nominal frequency. It is also noticed the losses slope is much better in the shaped coil compared to the high fill one. In other words, the losses increase slower in Coil III as the frequency increases. That is why Coil III is more suitable for higher frequency domain beside the advantage of direct cooling. Finally, the measured results are compared with the FEM simulation as shown in Fig. 21. In the 3D printed samples, there was an excellent match between the results because the strands have a well-defined location inside the slot. In the conventional multi-turn coil, there was a small mismatch between the losses which was mainly because of the randomness of the strand locations.

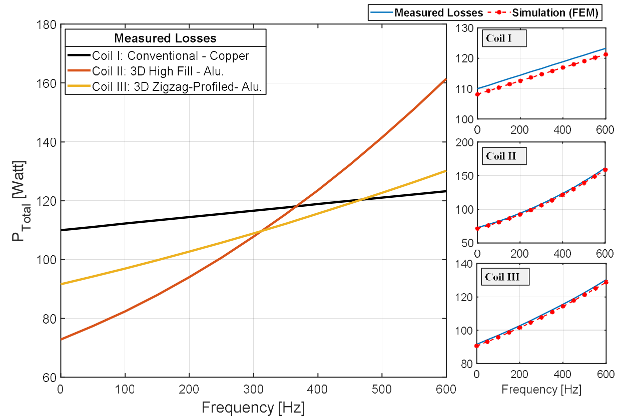

Fig. 21. Power losses measurements and validation for the conventional and 3D printed coils at the same ampere turn level.

VI. Thermal Performance Evaluation

A. *Influence of the Heat Exchanger Material*

Aiming for high thermal conductivity and low mass density, different materials are investigated for the zigzag heat exchanger as listed in Table III. The steady-state winding temperatures for the different materials are also estimated as shown in Fig. 22. As can be seen, the temperature decreases as the thermal conductivity increases. For instance, aluminum has high thermal conductivity. However, the mass density is relatively higher than most other options. Besides, the induced eddy current losses will be very high compared to the other non-conducting materials.

Table III.
Steady-State Winding Temperatures for Different Materials of the Heat Exchanger (*).

Material	Thermal conductivity [W/m K]	Mass density ** [kg/ m^3]	Winding temperature [°C]
Plastic (PA12)	0.3	1020	121
Epoxy (MC62)	1	1149	112
Carbon fiber (Standard 34 Msi)	9	1796	100
Thermoplastic (PA46)	14	1190	96
Stainless steel (316L)	15	7980	95
Carbon fiber (Thermasol WGCF20)	20	2900	92
Ceramic aluminum oxide	30	3950	88
Alumide63	90	1965	72
Ceramic silicon carbide	100	3160	69
Aluminum alloy	120	2670	65
(*) average coolant temperature of 20°C and 100 W losses in the winding			
(**) Mass density color:	1000-2000	2000-3000	3000-8000

To limit eddy currents, a custom alumide powder is engineered using AM technology with a good balance between weight as well as electrical and thermal conductivities. Normally, alumide is made from a mix of fine aluminum particles and a majority of polyamide powder (Nylon 12CF). In this study, the chemical composition is modified by increasing the aluminum powder to 63% to improve the thermal conductivity with a limited increase in the mass density. With the presence non-metallic particles, the new material has a mass density of 1965 kg/m^3, which is 26% lower than the aluminum. The modified material is also resistant to high temperatures up to 160°C. Using RLC meter, it is confirmed that the printed part has absolutely no electrical conductivity which helps in the mitigation of induced eddy currents. Finally, alumide material has a great printability to do some rapid prototyping. The only issue is that it has slightly higher porous compared to other metallic alternatives. Yet, the mechanical properties are fairly strong.

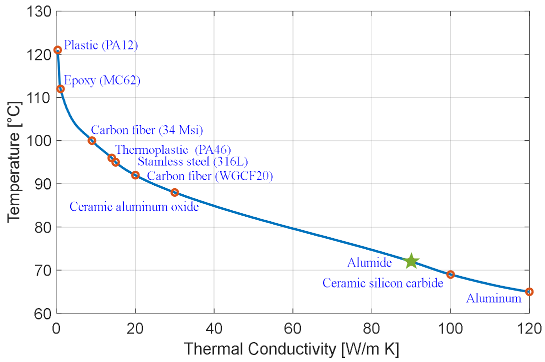

Fig. 22. Effect of the thermal conductivity of the heat exchanger material on the steady-state winding temperatures.

B. Mockup Assembly

To evaluate the thermal performance of the grooved-profile coils and the zigzag heat exchanger, two coils are printed using aluminum and three cooling channels are printed using alumide to cool each coil from both sides. The samples are assembled with the stator as shown in Fig. 23. The assembly sequence starts by inserting the 3D-printed coils radially. Then, all the cooling channels are inserted axially. Finally, two supports made from 3D printed carbon fiber are inserted axially to insure a very good contact for the side cooling channels. The main advantage of such design is that there is no need for partitioned stator. The cooling channel infiltrate perfectly between the coils with a very strong contact. A thermally conductive kapton tape is used as slot linear. Furthermore, a cooling terminal is designed and 3D printed to provide direct cooling for the windings as shown in Appendix A.

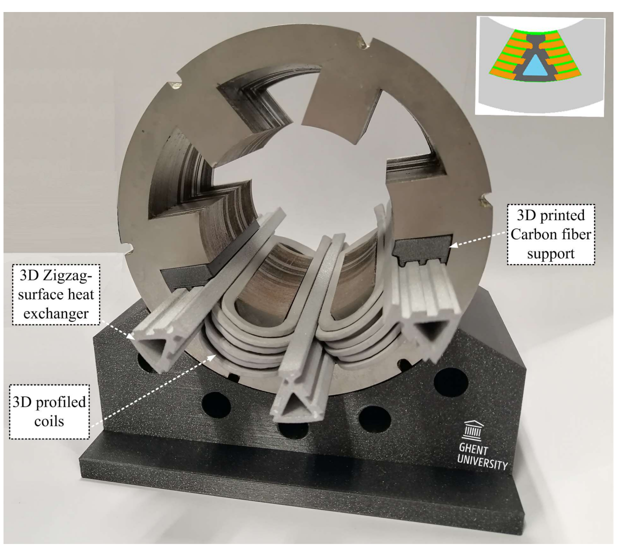

Fig. 23. Assembled stator with 3D grooved-profile coils and zigzag exchangers.

C. Performance Test

Here, the thermal performance of the test sample is evaluated with and without the cooling. Using a thermal camera, the steady state temperatures of the shaped coils are captured at a fixed ampere turns level before and after the cooling as shown in Fig. 24. As can be seen, without cooling, the coil temperature reached 107°C. However, with cooling, the temperature has remarkably fallen to only 37% of its value (39.3°C).

Furthermore, the ampere turns in the stator winding are pushed up to the thermal limit of the winding. In this case, a temperature limit is set to 155°C, and the cooling rate is maintained at the same value. For the reference case, this temperature limit was reached at a continuous ampere-turns of 910 AT. However, using the 3D alumide zigzag surface heat exchanger, the temperature limit was reached at a continuous ampere-turns of 1877 AT, which is more than 200% its value in the conventional windings.

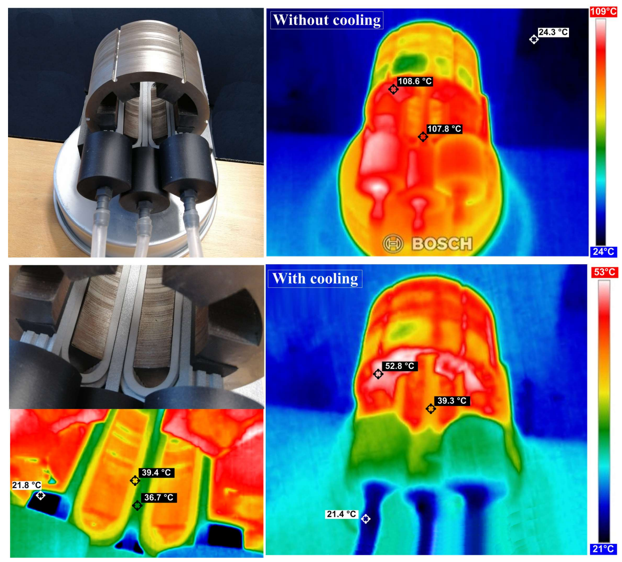

Fig. 24. Thermal profile of the 3D grooved-profile coils and zigzag exchangers with and without cooling.

D. Results Analysis

To sum up, a comparison between different coil cases are listed in Table IV. The conventional coils (Coil1) and the triangle-shaped direct cooling system are not as effective as expected in removing losses from windings. Instead, using a 3D coil with high fill factor (Coil2 or Coil3) and outer cooling jacket will provide a much better thermal performance and even lower weight (if aluminum coil is used; Coil3). Finally, the grooved-profile coil (Coil 4) along with the zigzag-surface direct cooling channel have the optimal thermal performance. Under the same ampere turns and cooling rate, Coil 4 has only half the temperature of the reference case (Coil I). That is why the proposed 3D shaped coil can push current limitations to significantly higher levels.

E. Hotspot Scanning and 3D End-Winding Cooling

In order to detect any hotspots in the 3D printed windings, a custom-designed cooling jacket is prototyped for the SRM motorette as shown in Fig. 25. The core is mounted on top of the cooling jacket using an interface of a thermally conductive heat transfer silicone paste (HTSP50T), which has a thermal conductivity of 3 W/m.K. Conventional ceramic insert pieces are used for the end windings shown in white color.

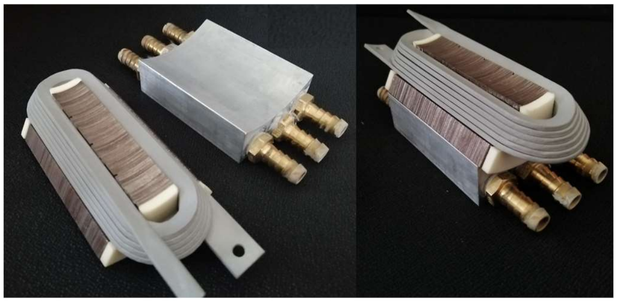

Fig. 25. Cooling jacket design for SRM motorette.

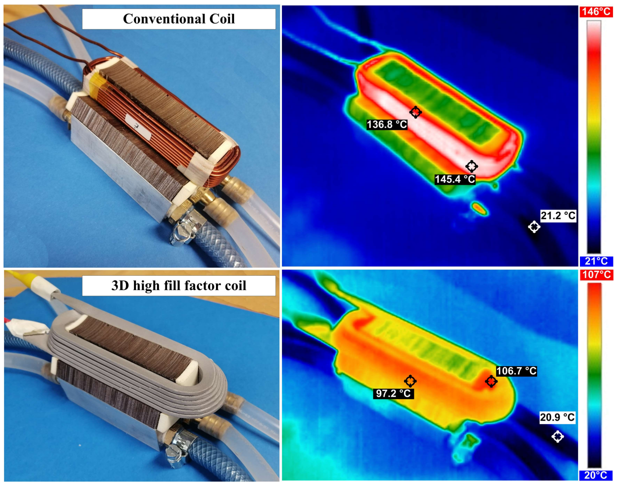

Fig. 26. Thermal profile of the 3D high fill coil compared to the conventional coil under the same ampere turns and cooling rate.

The thermal profile is measured for the 3D high fill coil and compared to the conventional coil under the same ampere turns and cooling rate as shown in Fig. 26. Clearly, the conventional coil has a much higher temperature profile. Also, a hotspot is detected at the end winding location for both coils. That is why a 3D end-winding insert is designed and printed using the same material as the zigzag cooling channel. The assembly of this end-winding insert with the 3D printed windings is shown in Fig. 27. The design is integrated with a cooling channel to ensure effective heat dissipation at the end winding location. The thermal profile is investigated again with the presence of the 3D end-winding insert as shown in Fig. 28. With the inclusion of this component, there is a significant temperature drop in the end winding and the hotspot is effectively eliminated. A comparison between the 3D printed coils and the reference coil in terms of peak temperature is shown in Fig. 29 under the same ampere turns and cooling rate. It is obvious that taking 3D end-winding cooling into account can help in reducing the peak temperature and eradicating any hotspots.

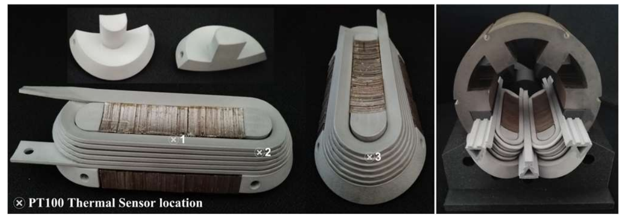

Fig. 27. Assembly of the 3D printed end-winding cooling insert with the 3D printed windings indicating PT100 locations.

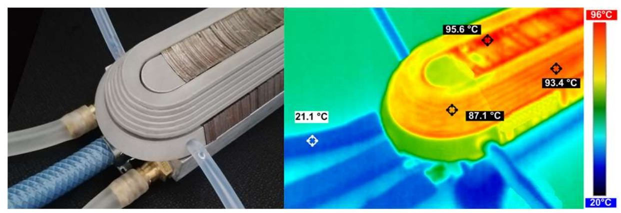

Fig. 28. Thermal profile of the 3D high fill coil with the additively-manufactured end-winding insert.

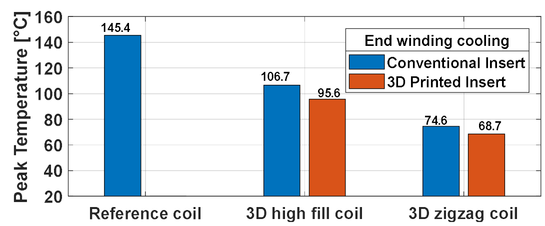

Fig. 29. Effect of 3D end-winding insert on the peak temperature of the thermal camera under the same ampere turns and cooling rate.

TABLE IV.
COMPARISON BETWEEN DIFFERENT COIL TOPOLOGIES

Coil	**Conventional**	**3D High Fill Cu.**	**3D High Fill Alu.**	**3D Profiled Alu.**
	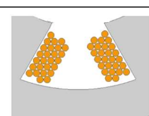	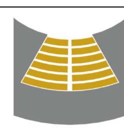	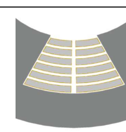	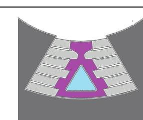
Number of Turns	26	6	6	6
Manufacturing Method	AWG 16 round wire	3D printed	3D printed	3D printed
Material	Copper	Copper	Aluminum	Aluminum
Fill factor	36.7%	73%	73%	58.6%
Weight	158.6 g (1.00 p.u.)	356.6 g (2.25 p.u.)	107 g (0.67 p.u.)	84.3 g (0.53 p.u.)
Losses at Nominal speed *[1]	1.00 p.u.	0.48 p.u. *[4]	0.73 p.u.	0.86 p.u.
Cooling Method	Direct cooling using conventional triangle tube	Outer water cooling Jacket	Outer water cooling Jacket	Direct cooling using 3D zigzag-surface heat exchanger
Max. Temp. @ same conditions*[2]	164.8°C	119.3°C	153.5°C	82.8°C
Ampere turn upper limit *[3]	910	1179 *[4]	1085	1877
Maximun Current density *[3]	10.47 A/mm^2	12.79 A/mm^2	11.04 A/mm^2	25.84 A/mm^2

*[1] At the same ampere turns (910 ATs) and 1 p.u.=112.2 W
*[2] At the same ampere turns (1080 ATs) and highest cooling rate h=1000 W/(m2.°C).
*[3] At the max. temperature limit (155°C) and highest cooling rate h=1000 W/(m2.°C).
*[4] Extrapolated value for a 3D printed copper coil

Lastly, an extra measurement is conducted employing PT100 sensors at three distinct positions within each coil, as previously highlighted in Fig. 27. The cooling system is effectively isolated from its surroundings to ensure that there is no heat loss to ambient. The mean temperature value is computed and outlined in Table V. The results have a very good alignment with the data taken by the thermal scanning camera. This agreement provides further validation for the accuracy of acquired results.

TABLE V.
MEAN TEMPERATURE VALUE MEASURED USING PT100 SENSORS

	Ref. Coil	3D HF Coil		3D Zig-zag Coil	
End-HX	N	N	Y	N	Y
Location 1	146.7°C	99.5°C	97.3°C	77.1°C	76.8°C
Location 2	151.3°C	107.2°C	94.4°C	77.4°C	71.9°C
Location 3	148.8°C	108.6°C	96.1°C	79.3°C	74.5°C
Mean value	148.93°C	105.1°C	95.9°C	77.97°C	74.4°C

End-HX: 3D printed end-winding heat exchanger
*(N) : No; without End-HX
*(Y) : Yes; with End-HX

VII. CONCLUSION

Enabled by 3D printing technology, this paper introduces new winding designs for low-loss lightweight electrical machines. Targeting high power density, the proposed designs combine between high electromagnetic and thermal performances. First, a coil with high fill factor is proposed using different materials (copper and aluminum). Both coils have better electrothermal performance due to their lower losses. Using SLM, this design is 3D printed using aluminum due to its remarkably lower weight. Secondly, a novel grooved-profile coil is proposed along with the zigzag-surface heat exchanger for in-slot direct cooling. With the increased contact surface area, this approach has the optimal thermal profile with at least 50% temperature drop. That allows for higher current carrying capacity. Different materials have been investigated for the shaped cooling channel, and a custom alumide material is engineered with a good balance between mass density and thermal conductivity. The proposed designs is 3D printed and the thermal performance is evaluated to verify its validity. Compared to the conventional copper coils, the new design has doubled the ampere turns limit with only 53% weight. Furthermore, 3D printed inserts are proposed to eliminate any hotspot at the end-windings. Overall, the proposed approaches highlight the unique capabilities of AM to overcome traditional manufacturability challenges and enable new design possibilities that contribute to the scalability, reliability, and effectiveness of electrical machines, making them more accessible for various applications.

APPENDIX A

Fig. 30 shows a 3D printed cooling terminal which was designed specifically for the zigzag cooling channel using lightweight carbon fiber material.

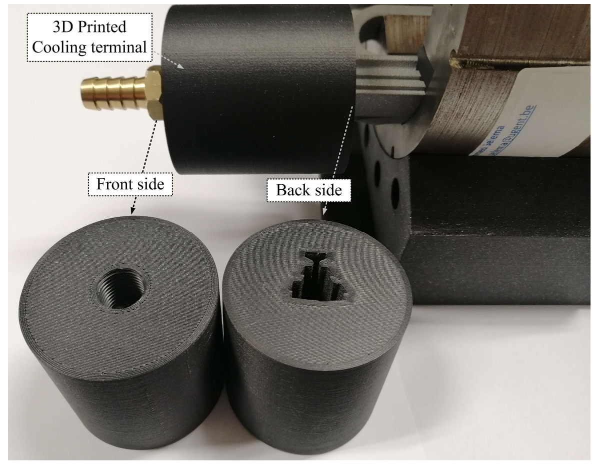

Fig. 30. Cooling terminal for the zigzag cooling channel.

ACKNOWLEDGMENT

This research is supported by the Research Foundation—Flanders (FWO) in the Strategic Basic Research project (No: S001721N) entitled Multi-Material Additive Manufacturing for Electrical Machines with increased performance (AM4EM).

Ahmed Selema received the M.Sc. degree in electrical engineering from Menoufia University, Egypt in 2018. In 2024, he received his Ph.D. degree in electromechanical engineering from Ghent University, Ghent, Belgium. Currently, he has been working as a research engineer in the Electrical Energy Lab (EELab) at Ghent University in a close collaboration with different industrial corporations in the EU. He is also a Corelab Member in Flanders Make, the strategic research center for the manufacturing industry in Flanders, Belgium. His research interests include electrical machines and drives, electromagnetics, material characterization, energy-efficient motor design, machine losses & cooling, and additive manufacturing. In these areas, he has authored or co-authored many papers in leading journals.

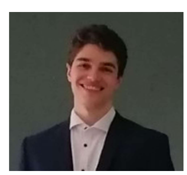

Joffrey Van Den Abbeele received his B.Sc. and M.Sc. degrees in electromechanical engineering from Ghent University, Belgium, in 2023. His M.Sc. research was conducted in the Electrical Energy Laboratory (EELab), Ghent University, under the supervision of Prof. Peter Sergeant and Ahmed Selema. His research interests include electric machines and additive manufacturing.

Mohamed N. Ibrahim received the Ph.D. degree in electromechanical engineering from Ghent University, Belgium in December 2017. In November 2008 and April 2018, he became a Teaching Assistant and an Assistant Professor (on leave) respectively at Electrical Engineering Department, Kafrelshiekh University, Egypt and since August 2023 he is an Associate Professor (on leave). Dr. Ibrahim worked as a Post-Doctoral researcher from December 2017 to November 2022, and he is currently working as Post-Doctoral assistant, all with the Department of Electromechanical, Systems and Metal Engineering, Ghent University, Belgium. His research interest focuses on electrical machines and drives for sustainability. He has over 100 publications and 1 patent in this research field. He is a senior Member of the IEEE.

Peter Sergeant received the M.Sc. degree in electromechanical engineering and the Ph.D. degree in engineering sciences from Ghent University, Ghent, Belgium, in 2001 and 2006, respectively. He became a Post-Doctoral Researcher at Ghent University in 2006 (Post-Doctoral Fellow of the Research Foundation-Flanders). Since 2012, he has been an Associate Professor at Ghent University. He is currently a Professor of electrical drives at Ghent University and a Core Lab Manager in the cluster motion products of Flanders Make. His current research domain is electrical machines and drives for industrial and for sustainable energy applications.

References

[1] N. Simpson and P. H. Mellor, "Additive manufacturing of shaped profile windings for minimal AC loss in gapped inductors," in *2017 IEEE International Electric Machines and Drives Conference (IEMDC)*, IEEE, May 2017, pp. 1–7. doi: 10.1109/IEMDC.2017.8002337.

[2] A. Selema, M. N. Ibrahim, and P. Sergeant, "Metal Additive Manufacturing for Electrical Machines: Technology Review and Latest Advancements," *Energies*, vol. 15, no. 3, p. 1076, Jan. 2022, doi: 10.3390/en15031076.

[3] S. Ayat, N. Simpson, B. Daguse, J. Rudolph, F. Lorenz, and D. Drury, "Design of Shaped-Profile Electrical Machine Windings for Multi-Material Additive Manufacture," in *2020 International Conference on Electrical Machines (ICEM)*, IEEE, Aug. 2020, pp. 1554–1559. doi: 10.1109/ICEM49940.2020.9270945.

[4] A. Selema *et al.*, "Evaluation of 3d-Printed Magnetic Materials for Additively-Manufactured Electrical Machines," *J. Magn. Magn. Mater.*, 2023, doi: 10.1016/j.jmmm.2023.170426.

[5] F. Wu and A. M. EL-Refaie, "Investigation of an Addtively-Manufactured Modular Permanent Magnet Machine for High Specific Power Design," in *2019 IEEE Energy Conversion Congress and Exposition (ECCE)*, IEEE, Sep. 2019, pp. 777–784. doi: 10.1109/ECCE.2019.8912763.

[6] S. Darius Gnanaraj, E. Gundabattini, and R. Raja Singh, "Materials for lightweight electric motors – a review," *IOP Conf. Ser. Mater. Sci. Eng.*, vol. 906, no. 1, p. 012020, Aug. 2020, doi: 10.1088/1757-899X/906/1/012020.

[7] M. Peter, J. Fleischer, F. S.-L. Blanc, and J.-P. Jastrzembski, "New conceptual lightweight design approaches for integrated manufacturing processes: Influence of alternative materials on the process chain of electric motor manufacturing," in *2013 3rd International Electric Drives Production Conference (EDPC)*, IEEE, Oct. 2013, pp. 1–6. doi: 10.1109/EDPC.2013.6689735.

[8] M. N. Ibrahim *et al.*, "Directly Cooled Windings in Switched Reluctance Machines," in *2020 International Conference on Electrical Machines (ICEM)*, IEEE, Aug. 2020, pp. 819–825. doi: 10.1109/ICEM49940.2020.9270925.

[9] H. Tiismus, A. Kallaste, T. Vaimann, and A. Rassõlkin, "State of the art of additively manufactured electromagnetic materials for topology optimized electrical machines," *Addit. Manuf.*, vol. 55, p. 102778, Jul. 2022, doi: 10.1016/j.addma.2022.102778.

[10] H. Chen, A. M. EL-Refaie, and N. A. O. Demerdash, "Flux-Switching Permanent Magnet Machines: A Review of Opportunities and Challenges—Part I: Fundamentals and Topologies," *IEEE Trans. Energy Convers.*, vol. 35, no. 2, pp. 684–698, Jun. 2020, doi: 10.1109/TEC.2019.2956600.

[11] A. Selema, M. N. Ibrahim, and P. Sergeant, "Additive Manufacturing for Electrical Machines: Opportunities and Challenges," in *Flanders Make: CMVPT Conference on Machines, Vehicles and Production Technology*, Gent, Belgium, 2022, p. 1. doi: 10.13140/RG.2.2.13028.65920.

[12] F. Wu and A. M. EL-Refaie, "Toward Additively Manufactured Electrical Machines: Opportunities and Challenges," *IEEE Trans. Ind. Appl.*, vol. 56, no. 2, pp. 1306–1320, Mar. 2020, doi: 10.1109/TIA.2019.2960250.

[13] A. Selema, M. N. Ibrahim, and P. Sergeant, "Non-Destructive Electromagnetic Evaluation of Material Degradation Due to Steel Cutting in a Fully Stacked Electrical Machine," *Energies*, vol. 15, no. 21, p. 7862, Oct. 2022, doi: 10.3390/en15217862.

[14] R. Hemmati, F. Wu, and A. El-Refaie, "Survey of Insulation Systems in Electrical Machines," in *2019 IEEE International Electric Machines & Drives Conference (IEMDC)*, IEEE, May 2019, pp. 2069–2076. doi: 10.1109/IEMDC.2019.8785099.

[15] Porsche AG; Amelia H., "Porsche Present 40% Lighter 3D Printed Electric Drive Housing," 2020. https://www.3dnatives.com/en/porsche-present-3d-printed-electric-drive-housing-261220204/ (accessed Dec. 18, 2022).

[16] J. Jaćimović *et al.*, "Net Shape 3D Printed NdFeB Permanent Magnet," *Adv. Eng. Mater.*, vol. 19, no. 8, p. 1700098, Aug. 2017, doi: 10.1002/adem.201700098.

[17] F. Bittner, J. Thielsch, and W.-G. Drossel, "Laser powder bed fusion of Nd–Fe–B permanent magnets," *Prog. Addit. Manuf.*, vol. 5, no. 1, pp. 3–9, Mar. 2020, doi: 10.1007/s40964-020-00117-7.

[18] A. Selema *et al.*, "Material Engineering of 3D-Printed Silicon Steel Alloys for the Next Generation of Electrical Machines and Sustainable Electromobility," *J. Magn. Magn. Mater.*, vol. 584, p. 171106, Oct. 2023, doi: 10.1016/j.jmmm.2023.171106.

[19] M. Beretta *et al.*, "Process optimization and characterization of dense pure copper parts produced by paste-based 3D micro-extrusion," *Addit. Manuf.*, p. 103670, Jun. 2023, doi: 10.1016/j.addma.2023.103670.

[20] A. Selema, M. N. Ibrahim, and P. Sergeant, "Additively Manufactured Ultralight Shaped-Profile Windings for HF Electrical Machines and Weight-Sensitive Applications," *IEEE Trans. Transp. Electrif.*, vol. 8, no. 4, pp. 4313–4324, Dec. 2022, doi: 10.1109/TTE.2022.3173126.

[21] F. Wu, A. EL-Refaie, and A. Al-Qarni, "Additively Manufactured Hollow Conductors Integrated With Heat Pipes: Design Tradeoffs and Hardware Demonstration," *IEEE Trans. Ind. Appl.*, vol. 57, no. 4, pp. 3632–3642, Jul. 2021, doi: 10.1109/TIA.2021.3076423.

[22] A. Selema, M. N. Ibrahim, and P. Sergeant, "Mitigation of High-Frequency Eddy Current Losses in Hairpin Winding Machines," *Machines*, vol. 10, no. 5, p. 328, Apr. 2022, doi: 10.3390/machines10050328.

[23] F. Wu, A. M. EL-Refaie, and A. Al-Qarni, "Additively Manufactured Hollow Conductors for High Specific Power Electrical Machines: Aluminum vs Copper," in *2021 IEEE Energy Conversion Congress and Exposition (ECCE)*, IEEE, Oct. 2021, pp. 4397–4404. doi: 10.1109/ECCE47101.2021.9595470.

[24] A. Selema, M. N. Ibrahim, and P. Sergeant, "Electrical Machines Winding Technology: Latest Advancements For Transportation Electrification," *Machines*, vol. 10, no. 5, 2022.

[25] N. Simpson, D. J. North, S. M. Collins, and P. H. Mellor, "Additive Manufacturing of Shaped Profile Windings for Minimal AC Loss in Electrical Machines," *IEEE Trans. Ind. Appl.*, vol. 56, no. 3, pp. 2510–2519, May 2020, doi: 10.1109/TIA.2020.2975763.

[26] A. Selema, M. Gulec, M. N. Ibrahim, R. Sprangers, and P. Sergeant, "Selection of Magnet Wire Topologies With Reduced AC Losses for the Windings of Electric Drivetrains," *IEEE Access*, vol. 10, pp. 121531–121546, 2022, doi: 10.1109/ACCESS.2022.3222773.

[27] N. Simpson, S. P. Munagala, A. Catania, F. Derguti, and P. H. Mellor, "Functionally Graded Electrical Windings Enabled by Additive Manufacturing," in *2022 International Conference on Electrical Machines (ICEM)*, IEEE, Sep. 2022, pp. 1477–1483. doi: 10.1109/ICEM51905.2022.9910912.

[28] A. Selema, M. N. Ibrahim, R. Sprangers, and P. Sergeant, "Effect of Using Different Types of Magnet Wires on the AC Losses of Electrical Machine Windings," in *2021 IEEE International Electric Machines & Drives Conference (IEMDC)*, IEEE, May 2021, pp. 1–5. doi: 10.1109/IEMDC47953.2021.9449507.

[29] P. Mellor, J. Hoole, and N. Simpson, "Computationally efficient

prediction of statistical variance in the AC losses of multi-stranded windings," in *2021 IEEE Energy Conversion Congress and Exposition (ECCE)*, IEEE, Oct. 2021, pp. 3887–3894. doi: 10.1109/ECCE47101.2021.9595867.

[30] H. Vansompel and P. Sergeant, "Extended End-Winding Cooling Insert for High Power Density Electric Machines With Concentrated Windings," *IEEE Trans. Energy Convers.*, vol. 35, no. 2, pp. 948–955, Jun. 2020, doi: 10.1109/TEC.2019.2953577.

[31] N. A. Rahman, E. Bostanci, and B. Fahimi, "Thermal analysis of switched reluctance motor with direct in-winding cooling system," in *2016 IEEE Conference on Electromagnetic Field Computation (CEFC)*, IEEE, Nov. 2016, pp. 1–1. doi: 10.1109/CEFC.2016.7816110.

[32] S. M. Ammar and C. W. Park, "Validation of the Gnielinski correlation for evaluation of heat transfer coefficient of enhanced tubes by non-linear regression model: An experimental study of absorption refrigeration system," *Int. Commun. Heat Mass Transf.*, vol. 118, p. 104819, Nov. 2020, doi: 10.1016/j.icheatmasstransfer.2020.104819.

[33] C. Silbernagel, I. Ashcroft, P. Dickens, and M. Galea, "Electrical resistivity of additively manufactured AlSi10Mg for use in electric motors," *Addit. Manuf.*, vol. 21, pp. 395–403, May 2018, doi: 10.1016/j.addma.2018.03.027.

[34] M. Zhu, Z. Jian, G. Yang, and Y. Zhou, "Effects of T6 heat treatment on the microstructure, tensile properties, and fracture behavior of the modified A356 alloys," *Mater. Des.*, vol. 36, pp. 243–249, Apr. 2012, doi: 10.1016/j.matdes.2011.11.018.